

2019-01-17

Beach recovery from extreme storm activity during the 2013/14 winter along the Atlantic coast of Europe

Dodet, G

<http://hdl.handle.net/10026.1/12865>

10.1002/esp.4500

Earth Surface Processes and Landforms

Wiley

All content in PEARL is protected by copyright law. Author manuscripts are made available in accordance with publisher policies. Please cite only the published version using the details provided on the item record or document. In the absence of an open licence (e.g. Creative Commons), permissions for further reuse of content should be sought from the publisher or author.

1 Beach recovery from extreme storm activity
2 during the 2013/14 winter along the Atlantic coast
3 of Europe

4 Guillaume Dodet¹, Bruno Castelle^{2,3}, Gerd Masselink⁴, Tim Scott⁴,
Mark Davidson⁴, France Floc'h⁵, Derek Jackson⁶, Serge Suanez¹

5 ¹Université de Bretagne Occidentale, CNRS, UMR LETG-6554,
6 Institut Universitaire Européen de la Mer, Plouzané, France,
7 guillaume.dodet@univ-brest.fr

8 ²CNRS, UMR EPOC, Pessac, France

9 ³Université de Bordeaux, UMR EPOC, Pessac, France

10 ⁴Coastal Processes Research Group, School of Biological and Marine
11 Sciences, Plymouth University, Plymouth, UK

12 ⁵Géosciences Océan UMR 6538 CNRS, Institut Universitaire
13 Européen de la Mer (UBO), Plouzané, France

14 ⁶Centre for Coastal and Marine Research, School of Geography and
15 Environmental Sciences, Ulster University, Coleraine, UK

16 **Abstract**

17 The storm sequence of the 2013/14 winter left many beaches along the At-
18 lantic coast of Europe in their most eroded state for decades. Understanding
19 how beaches recover from such extreme events is essential for coastal man-
20 agers, especially in light of potential increases in storminess due to climate
21 change. Here we analyze a unique dataset of decadal beach morphological
22 changes along the west coast of Europe to investigate the post-2013/14-
23 winter recovery. We show that the recovery signature is site-specific and
24 multi-annual, with one studied beach fully recovered after two years, and
25 the others only partially recovered after four years. During the recovery
26 phase, winter waves primarily control the timescales of beach recovery, as

energetic winter stall the recovery process while moderate winter accelerate it. This inter-annual variability is well correlated with climate indices. On exposed beaches, an equilibrium model showed significant skill in reproducing the post-storm recovery and thus can be used to investigate the recovery process in more details.

1 Introduction

Sand and gravel beaches may undergo dramatic erosion and recession during sequences of extreme storm wave events (Ferreira, 2006), leaving them in a state of morphological dis-equilibrium. A phase of ‘recovery’ towards pre-storm sediment volume is then a natural morphodynamic response to this depleted state (Brenner et al., 2018). Because the rates of recovery depend on the magnitude of the storm-induced changes, the subsequent hydrodynamic conditions, the sediment availability and the geological setting, predicting the time until full recovery is achieved (if ever) is challenging. Given the current predictions of climate change, the acceleration of sea level rise (Cazenave and Cozannet, 2014) and the potential intensification of storminess (Donat et al., 2011) will increase extreme water levels and may increase the frequency of winter storms in the near future (IPCC AR5 Pachauri et al., 2014). Hence, addressing the timescales of beach recovery to extreme storm winters, such as the 2013/14 winter, can provide a measure of coastal resilience in a changing climate.

Beach recovery from severe storms has been shown to spread over years to decades (Morton et al., 1994; Houser and Hamilton, 2009; Castelle et al., 2017a). Since beach morphodynamics are often characterized by a significant seasonal signal (Aubrey, 1979; Masselink and Pattiaratchi, 2001; Davidson and Turner, 2009), the long-term recovery signature is often hard to detect within the shorter-term fluctuations (Thom and Hall, 1991; Stephan et al., 2015). Therefore, high-frequency monitoring of beach morphology over long time periods is crucial to understand better storm recovery (Turner et al., 2016). Unfortunately, such monitoring programmes are scarce, and the few available data sets have been used mostly to characterize extreme storm responses (Scott et al., 2016; Barnard et al., 2017), investigate the parameters controlling beach morphological changes (Yates et al., 2011) and develop semi-empirical equilibrium models able to reproduce these morpholog-

ical changes (Davidson and Turner, 2009; Yates et al., 2009; Splinter et al., 2014). However, ongoing field monitoring programmes in France and UK have recently shed some lights on the key mechanisms involved during post-storm recovery (Scott et al., 2016; Castelle et al., 2017a; Burvingt et al., 2018). Scott et al. [2016], investigated the morphological changes at three contrasting sites in SW England during the two years that followed the extreme 2013/14 winter. They found that the recovery mechanisms and timescales were highly dependent on the site characteristics, and that high-energy wave events were essential for the recovery of sediments. Burvingt et al. (2018), found that for a number of very similar beaches in SW England, recovery from the 2013/14 storm was regionally-coherent, multi-annual (>3 years), and mainly controlled by winter-wave conditions. Castelle et al. (2017a) investigated how the beach-dune system of an exposed site in SW France recovered from winter 2013/14 and found that only after 1.5 year the beach-dune system almost fully recovered to its pre-winter volume. These site-specific recovery rates highlight the need to conduct studies at broader scales, including different beaches, in order to investigate the key parameters that control the recovery timescales.

During the 2013/14 winter, a highly unusual sequence of extratropical storms crossed the North-East Atlantic region. This winter was the most energetic winter along the Atlantic coast of Europe since at least 1948 (Masselink et al., 2016a), and most of the west European coastline was severely impacted (Castelle et al., 2015; Blaise et al., 2015; Masselink et al., 2016b; Autret et al., 2016). Although winter waves are known to be well correlated with the North Atlantic Oscillation (NAO) index at high latitudes (Bacon and Carter, 1993; Dodet et al., 2010; Bromirski and Cayan, 2015), this exceptional winter was not associated with a particularly high NAO. Castelle et al. (2017b) computed a new climate index based on the sea level pressure gradient between Ireland and the Canary Islands: the West Europe Pressure Anomaly (WEPA). They showed that the 2013/14 winter was associated with the highest WEPA over 1948-2016, which reflects an intensified and southward shift of the sea level pressure difference between the Icelandic low and the Azores high, driving severe storms that funnel high-energy waves toward western Europe southward of 52°N .

In this paper, we investigate the post-2013/14 winter recovery of five beaches along the west coast of Europe; these are the same beaches for which

the 2013/14 storm response was reported in Masselink et al. (2016a). Our objectives are threefold: 1) to obtain insight into the time scale of recovery for this extreme event for the different locations; 2) to explain the difference in observed recovery time scales by identifying the key factors involved; and 3) to determine extent to which extreme erosion and recovery processes can be modeled using present equilibrium models.

2 Methods

2.1 Wave Modeling

Two wave model hindcasts were used in this study. First, a large-scale and low-resolution model was used to characterize the wave climate in the North-East Atlantic, and more particularly the N-S differences in the wave forcing along the west coast of Europe. For this purpose, the spectral wave model WAVEWATCH III V4.18 (WW3, Tolman, 2014) was implemented on a 0.5° resolution grid covering the North Atlantic Ocean and forced with the 6-hourly wind fields of the NCEP/NCAR Global Reanalysis Project (Kalnay et al., 1996) from January 1948 to December 2017. Time series of significant wave heights (H_s) were extracted at three deep-water locations (shown in Figure 1): north west of Ireland (10.0°W ; 56.0°N), in the Bay of Biscay (7.0°W ; 47.0°N), and west of Portugal (11.0°W ; 40.0°N). Details of the model setup and validation of the simulations with wave buoy observations can be found in Masselink et al. (2016a). Second, a smaller scale, high-resolution model was used to simulate the wave conditions close to the breaking point at each study site. Indeed, the offshore wave conditions simulated with the 0.5° model were not necessarily representative of nearshore wave conditions at some of the sheltered study locations. For this purpose we used a WW3 hindcast (1992-2017) implemented on an unstructured grid with a resolution increasing from 10 km offshore to 200 m in the coastal region extending from north of Spain to south of Ireland (Boudière et al., 2013). This model has been extensively validated with directional buoy and satellite altimeter and showed excellent skill, with correlation coefficients of more than 0.94 and root-mean square errors less than 0.2 m for the whole set of validation points (Boudière et al., 2013; Ardhuin et al., 2012). Model outputs were extracted for each study site at a distance less than 6 km from the coast, in water depths of 20-35 m. Seasonal means were computed for

131 the winter (DJFM) and for the spring-summer-autumn (AMJJASON).

132 2.2 Study Sites and Beach Volumes

133 Five beaches along the Atlantic coast of Europe were surveyed on a monthly
134 basis for more than 10 years. This data set represents one of the most com-
135 plete series of beach profiles along western Europe. The location of the study
136 beaches are shown in Figure 1, and the morphological characteristics of the
137 study sites are given in Table 1. Additional information on the survey meth-
138 ods can be found in Masselink et al. (2016a). Since Slapton Sands displayed
139 a strong alongshore variability in beach profile evolution, two representative
140 beach profiles were analyzed separately, corresponding to the middle (SP10)
141 and northern end (SP18) of the beach.

142 The extension of this data set to November 2017 was used to investigate
143 the morphological recovery of the beaches four years after the exceptionnal
144 2013/14 winter. For this purpose, the beach volume above mean sea level
145 (V) was computed for each site, with no upper limit set except at Perran-
146 porth where data was not collected for elevations higher than approximately
147 3 m above MSL. Beach volume V , which therefore includes the dune system
148 at Vougot, Porsmilin and Truc Vert, was assumed to provide an accurate
149 and integrated measure of the beach system change (see left-hand panels
150 of Fig. 4 in Masselink et al. (2016a)). Then, the beach volume changes
151 ($|dV|$) were divided into four components: 1) beach volume change caused
152 by the long-term trend computed over the period prior to the 2013/14 win-
153 ter; 2) seasonal signal, computed from the detrended signal as the aver-
154 age annual difference between the maximum and minimum beach volume
155 ($\frac{1}{N} \sum_{i=1}^N |V_{i,max} - V_{i,min}|$, where i is a yearly increment and N is the num-
156 ber of years in the time series); 3) 2013/14 winter response, computed as
157 the difference in beach volume prior to and after the 2013/14 winter; and 4)
158 post-2013/14 winter recovery, computed as the difference in beach volumes
159 between April 2014 and November 2017. Note that the long-term trend and
160 the seasonal contribution were only computed over the time period prior to
161 the 2013/14 winter to ensure these signals were not affected by the 2013/14
162 winter storm response. Rates of beach volume changes (dV/dt) were com-
163 puted for the winter and spring-summer-autumn from the observations clos-
164 est in time to December 1 and April 1. When no observations were available
165 within two weeks before or after these dates, the corresponding dV/dt was

not computed. In the remaining of the paper, the percentage of recovery is computed as the beach volume changes associated with the post-storm recovery relative to the 2013/14 winter response, as defined above (components 3 and 4).

2.3 Beach Equilibrium Modeling

To assess whether an equilibrium-based model can be used to forecast beach recovery to an extreme storm event, the ShoreFor model (Davidson et al., 2013) was applied. This semi-empirical model predicts shoreface erosion when the wave conditions are more energetic than the equilibrium conditions (computed as a weighted average of past wave conditions) and vice-versa, and the magnitude of change is proportional to the incident wave power and degree of disequilibrium. The model has two free parameters that require calibration: a disequilibrium term and a linear trend term. The linear trend term crudely accounts for all processes other than wave-driven cross-shore transport, including longshore sediment transport processes. The reader is referred to Davidson et al. (2013) for a full description of the model. For all sites, the model was calibrated with the period of observations prior to the 2013/14 winter, and validated during the remaining period that includes the 2013/14 winter storm response and the subsequent 4-year recovery period. The model skill was assessed with the correlation coefficient (R) between observed (x) and simulated (x_m) beach volumes, the root-mean-square error ($RMSE$), and the root-mean-square error normalized by the observed variance prior to the 2013/14 winter ($NRMSE$). Because records with a significant linear trend, possibly induced by longshore transport processes or other net source/sinks of sediments, sometimes show high model skill solely attributable to the linear trend component in the model, the model skill was also assessed using the Brier Skill Score (BSS), which allows comparison of the model residuals with a suitable baseline (x_b), taken here as the linear trend component of the model. The BSS is computed as follows:

$$BSS = 1 - \frac{\sum (x - x_m)^2}{\sum (x - x_b)^2} \quad (1)$$

A positive BSS indicates an improvement relative to the baseline, and values greater than 0.0, 0.3, 0.6, 0.8 are typically described as ‘poor’, ‘fair’, ‘good’, ‘excellent’, respectively (van Rijn et al., 2003; Sutherland et al., 2004). Note

that this modelling approach does not resolve long-shore transport processes and is thus expected to show poor skills when applied to environments dominated by long-shore transport.

3 Results

3.1 Modeled Wave Conditions

The wave conditions simulated with the regional model over the period 2002-2017 for the north-west of Ireland, the Bay of Biscay, and west of Portugal are shown in Figure 1. A clear seasonal signal characterizes the three time series, with winter-mean H_s much larger than spring-summer-autumn-mean H_s (56 % greater on average, and up to 120 % greater locally). Moreover, the winter-mean values display strong inter-annual variability ($\sigma/\overline{H_s} = 0.12$ on average, where σ is the standard deviation, and $\overline{H_s}$ is the long-term mean H_s), whereas the spring-summer-autumn-mean values display much lower inter-annual variability ($\sigma/\overline{H_s} = 0.06$). The consequence of these fluctuations is that, contrary to spring-summer-autumn means, the winter-mean H_s may differ significantly from one year to another. For instance, the largest winter-mean H_s in the Bay of Biscay and west of Portugal occurred during the 2013/14 winter, and they were approximately 35 % greater than the long-term mean winter H_s . During the following winter, wave conditions were moderate in the Bay of Biscay and west of Portugal, but obtained their maximum north of Ireland. These trends were inverted during the 2015/16 winter as the winter-mean H_s was very large in the Bay of Biscay and west of Portugal, but moderate north of Ireland. The most recent 2016/17 winter was moderate in all three regions. This inter-annual variability of winter-mean H_s was shown to be significantly correlated with the WEPA index southward of 52°N (Castelle et al., 2017b) and with the NAO index further north (Bacon and Carter, 1993; Dodet et al., 2010; Bromirski and Cayan, 2015). This dependence on NAO and WEPA indices is confirmed by our results, with the highest (respectively lowest) NAO during the 2014/15 (respectively 2009/10) winter correlating with the maximum (respectively minimum) H_s north of Ireland for this winter, and the two highest WEPA during the 2013/14 and 2015/16 winters correlating with the maximum H_s in the Bay of Biscay and west of Portugal for these winters. Correlation coefficients between the winter-mean H_s and the NAO and WEPA indices are shown on

232 Figure 1.

233 3.2 Beach Recovery from the 2013/14 winter

234 Figure 2 shows the complete time series of beach volume changes for the
235 six beach profiles (left-hand column), and the relative contributions of the
236 long-term trend, seasonal signal, 2013/14 winter response and post-2013/14
237 winter recovery (right-hand column). Contrasting behaviors are observed.
238 First, the most exposed sites, Perranporth and Truc Vert, suffered unprece-
239 dented erosion during the 2013/14 winter. Yet, after two years, Truc Vert
240 had fully recovered, while Perranporth had only recovered 70 % after four
241 years. The major difference in these recovery rates occurred during the year
242 2015. From early February to mid-December 2015, the beach volumes at
243 Truc Vert increased steadily and the beach recovered more than 80 % of the
244 sediments lost during the 2013/14 winter within a span of 10 months (see
245 Castelle et al., 2017a, for details). At Perranporth, the beach was in a re-
246 covery phase for a shorter period of time - from late-March to November
247 2015 - regaining only 40 % of the sediments lost during the 2013/14 winter.
248 This contrasting response can be directly related to the difference in wave
249 conditions in January, March, November and December 2015 that were par-
250 ticularly stormy at Perranporth (H_s was 60 % higher than the annual mean
251 at Perranporth and only 30 % higher at TrucVert). Porsmilin was also in its
252 most eroded state after the 2013/14 winter, but after two years the beach had
253 recovered by almost 80 %. This fast recovery was fostered by the relatively
254 calm wave conditions during the 2014/15 winter that did not cause much ero-
255 sion at this sheltered site. The beach volumes at Vougot are dominated by
256 a decreasing long-term trend. Although the coastal dune retreated by more
257 than 5 m during the 2013/14 winter, the sediment remained in the intertidal
258 zone and the beach volume actually increased slightly. After four years, the
259 dune had prograded back by approximately 3 m. At Slapton Sands, the cen-
260 tral (SP10) and east (SP18) profiles showed opposite behaviors as a result
261 of beach rotation processes. An additional factor that could explain the dif-
262 ference in recovery rates is the difference in tidal range. Large tidal range
263 cause shorter residence time within the upper intertidal profile and subse-
264 quently longer morphological response times. However, no clear conclusion
265 on this process was drawn from our data set, since both slow (Perranporth)
266 and fast (Porsmilin) responses were observed on macrotidal beaches.

267 To investigate the relationship between beach dynamics and incident
 268 wave conditions, the rates of beach volume changes (dV/dt) during the win-
 269 ter season and during the spring-summer-autumn season are compared to the
 270 respective seasonal wave energy anomalies, i.e., the deviation of the season-
 271 mean wave energy from the long-term (1992–2017) annual mean wave energy
 272 \bar{E} (Figure 3). Overall, dV/dt displays much greater variability during the
 273 winter season than during the rest of the year. At Perranporth, Pormsilin
 274 and Truc Vert, the winter-mean variability of dV/dt is clearly controlled by
 275 the wave conditions ($0.58 < R^2 < 0.65$). The near-zero intercept of the lin-
 276 ear trends indicates that the beach profile is close to equilibrium when the
 277 winter-mean E is close to the long-term yearly mean \bar{E} . Although winter
 278 wave conditions are associated mostly with erosive conditions, low winter-
 279 mean E can cause beach accretion. For instance, during the 2009/10 winter,
 280 the wave conditions were particularly calm north of 50°N , due to a very low
 281 NAO and a modest WEPA, and the sand volume at Perranporth increased
 282 by $26 \text{ m}^3/\text{m}$. For the spring-summer-autumn season, correlations between
 283 dV/dt and wave energy anomalies are much lower and mostly insignificant at
 284 the 95 % level. One reason is that dV/dt cannot progressively increase when
 285 E tends towards zero; very low energy waves contribute less to onshore sedi-
 286 ment transport than low to moderate energy waves, hence limiting recovery
 287 (Hoefel and Elgar, 2003; Fernández-Mora et al., 2015). At Slapton Sands
 288 profiles SP10 and SP18, the winter-mean dV/dt is also strongly controlled
 289 by the wave conditions; however, the correlations have opposite signs as a
 290 result of beach rotation. Wiggins et al. (2017) showed very high correlations
 291 between beach volume changes and the directional wave power at Slapton
 292 Sands, and the insignificant correlations for the spring-summer-autumn sea-
 293 son are probably because the beach changes were mostly controlled by the
 294 wave direction and not by the wave energy. At Vougot, there is no correla-
 295 tion between dV/dt and the wave conditions. Indeed, the behavior of the
 296 beach-dune system is severely impacted by the presence of a jetty at the
 297 north-eastern end of the beach. Since its construction in 1974 the beach has
 298 continually lost sediment, independent of the wave conditions (Suanes et al.,
 299 2010).

300 Finally, the beach volume changes were compared with the results of
 301 the beach equilibrium model ShoreFor (Davidson et al., 2013) to assess the
 302 amount of variance attributable to cross-shore sediment transport and to

303 antecedent wave conditions. The analysis completed thus far treats each
 304 year independently, while ShoreFor accounts for antecedent wave conditions.
 305 It is therefore expected to explain more of the variability in the beach volume
 306 at the cross-shore dominated beaches through the disequilibrium term than a
 307 simple model based on a linear correlation between dV/dt and the mean wave
 308 height. Figure 4 shows the observed versus simulated beach volume changes
 309 using the ShoreFor model, as well as the error metrics $RMSE$, $NRMSE$, R ,
 310 and BSS . Inspection of this figure reveals that Perranporth and Truc Vert
 311 have low $NRMSE$ ($<5\%$) and ‘excellent’ BSS , indicating that ShoreFor is
 312 able to reproduce fairly well the storm response and subsequent recovery, and
 313 this variance is mostly induced by cross-shore processes. With a $NRMSE <$
 314 15% and a ‘fair’ BSS , ShoreFor results are moderate, and beach volume
 315 changes at Porsmilin can also be considered as dominated by cross-shore
 316 processes. Conversely, the negative BSS scores at Slapton SP18 and Vougot
 317 indicate that the model performs worse than predictions based on the long-
 318 term trend only. At Slapton SP10, both R and the BSS are relatively high;
 319 however, the very large $NRMSE$ (270.4%) reveals that some significant
 320 processes are ignored by the model. Hence, Vougot and Slapton Sands cannot
 321 be considered as being dominated by cross-shore sediment transport and
 322 more advanced numerical models, including longshore sediment transport,
 323 must be applied to reproduce extreme storm response and recovery at these
 324 sites.

325 4 Discussion and Conclusions

326 The analysis of decadal beach morphological changes along the Atlantic coast
 327 of Europe revealed that the dynamics of beaches exposed to a pronounced
 328 seasonal wave climate are controlled by processes operating over a variety
 329 of time scales. In decreasing order these time scales are: long-term trends
 330 (decade), post-storm recovery (years), seasonal changes (months), and storm
 331 response (days). Total beach dynamics represent the sum of these compo-
 332 nents and for different beaches the relative contribution of each of these
 333 components varies significantly, making beach volume predictions challeng-
 334 ing and site-specific. Moreover, beach recovery is conventionally thought to
 335 be a process that occurs during the calm summer months. However, although
 336 beaches do recover during the spring-summer-autumn period at modest and

337 relatively steady rates (not much inter-annual variability), winter conditions
 338 that primarily control the time it takes for beaches to recover from extreme
 339 erosion. Highly energetic winters stall or even reverse the recovery process,
 340 whereas calm winters continue the recovery process. Therefore, climate in-
 341 dices such as NAO and WEPA, which are known to explain a significant
 342 part of the inter-annual variability of winter wave conditions in the North-
 343 East Atlantic (Dodet et al., 2010; Castelle et al., 2017b), are well correlated
 344 with the recovery process. For instance, the most exposed sites Perranporth
 345 and Truc Vert required calm winter conditions to recover from the 2013/14
 346 winter erosion, which correspond to negative values of WEPA. This was the
 347 case for the 2014/15 and 2016/17 winters (Figure 1), during which these
 348 beaches showed relatively small rates of volume changes (Figure 3). The
 349 recovery of these beaches could have been accelerated if the 2015/16 winter,
 350 which was characterized by a high WEPA value, had not caused severe ero-
 351 sion and slowed down the recovery process (Figure 3). At Slapton Sands,
 352 easterlies have been shown to foster beach recovery following storm erosion
 353 by (southwesterly) Atlantic storms, and these are promoted in this region by
 354 negative NAO values (Wiggins et al., 2017). The systematic positive NAO
 355 winters that followed the 2013/14 winter, and the prevailing southwesterly
 356 wave conditions, limited beach recovery at this site.

357 Predicting long-term beach morphological change is of great importance
 358 to coastal managers. While process-based morphodynamic modeling sys-
 359 tems are valuable tools to simulate the morphological impact of single storm
 360 events (e.g. McCall et al., 2010; Almeida et al., 2017), their computational
 361 cost prevents their application to multi-annual or even inter-annual morpho-
 362 logical changes. In contrast, beach equilibrium models are computationally
 363 cheap and can be applied for investigating long-term morphological changes
 364 (e.g. Yates et al., 2011; Splinter et al., 2014). For cross-shore transport domi-
 365 nated sites, the ShoreFor model calibrated with topographic data prior to the
 366 winter 2013/14 and forced with nearshore wave conditions simulated with
 367 a high-resolution model showed significant skills in reproducing the strong
 368 erosion caused by the extreme 2013/14 winter and the recovery phase that
 369 followed, particularly at Truc Vert and Perranporth. Not surprisingly, Shore-
 370 For shows poor skill at sites where longshore processes and resulting beach
 371 rotation signal dominate shoreline variability, i.e. at Vougot and Slapton.
 372 At Porsmilin, due to the small elevation of the artificial embankments at

the top of the upper beach, a significant fraction of the sediment lost during the winter 2013/14 was deposited further inland during washover events. We believe this may explain why the model failed in reproducing accurately the volume changes during and after the winter. Semi-empirical models combining the equilibrium-based behaviour owing to variability in incident wave energy with longshore processes are scarce and still under development (Vitousek et al., 2017; Robinet et al., 2017). Although out of scope of this study, the further development of these models will extend the domain of applicability of shoreline change models, making it possible to address coastal vulnerability and resilience in the context of climate change. Mentaschi et al. (2017) analyzed projection of extreme wave energy fluxes under a high emission scenario (Representative Concentration Pathways 8.5) and showed a significant increase in the 100-year return level of wave energy fluxes for the southern hemisphere and for some regions of the northern hemisphere. It is very likely that such changes in the wave climate will significantly impact beach morphodynamics at both event scales (storm response) and long-term scales (post-storm recovery), which will require accurate predictions for implementing coastal adaptation strategies.

Acknowledgments

This work was supported financially by the French Naval Oceanographic and Hydrographic Department (Shom) through the research program PROTEVS (12CR6), and by the "Laboratoire d'Excellence" LabexMER (ANR-10-LABX-19-01) program. BC was funded by the SONO (ANR-17-CE01-0014) and CHIPO (ANR-14-ASTR-0004) projects of the *Agence Nationale de la Recherche* (ANR) and by the AST "Evenements extremes" of the *Observatoire Aquitain des Sciences de l'Univers* (OASU). GM and TS were funded by the NERC BLUE-coast project (NE/N015525/1). The French sites Vougot, Porsmilin and Truc Vert are monitoring sites of the Service National d'Observation (SNO) DYNALIT labelled by CNRS-INSU and part of the French Research Infrastructure ILICO. The authors would like to thank the very many colleagues, postdocs, field technicians and PhD students involved in the beach profile data collection. We acknowledge NCEP/NCAR and Ifremer institutes for providing the wind field reanalysis and the wave hindcast, respectively. The topographic and wave data that were used for

the analysis are provided as supplementary material of this paper.

References

- Almeida, L. P., Masselink, G., McCall, R., and Russell, P. (2017). Storm
overwash of a gravel barrier: Field measurements and XBeach-G mod-
elling. *Coastal Engineering*, 120:22–35.
- Ardhuin, F., Roland, A., Dumas, F., Bennis, A.-C., Sentchev, A., Forget, P.,
Wolf, J., Girard, F., Osuna, P., and Benoit, M. (2012). Numerical Wave
Modeling in Conditions with Strong Currents: Dissipation, Refraction,
and Relative Wind. *Journal of Physical Oceanography*, 42(12):2101–2120.
- Aubrey, D. G. (1979). Seasonal patterns of onshore/offshore sediment move-
ment. *Journal of Geophysical Research: Oceans*, 84(C10):6347–6354.
- Autret, R., Dodet, G., Fichaut, B., Suanez, S., David, L., Leckler, F., Ard-
huin, F., Ammann, J., Grandjean, P., Allemand, P., and Filipot, J.-F.
(2016). A comprehensive hydro-geomorphic study of cliff-top storm de-
posits on Banneg Island during winter 2013–2014. *Marine Geology*, 382:37–
55.
- Bacon, S. and Carter, D. J. T. (1993). A connection between mean wave
height and atmospheric pressure gradient in the North Atlantic. *Interna-
tional Journal of Climatology*, 13(4):423–436.
- Barnard, P. L., Hoover, D., Hubbard, D. M., Snyder, A., Ludka, B. C., Allan,
J., Kaminsky, G. M., Ruggiero, P., Gallien, T. W., Gabel, L., McCandless,
D., Weiner, H. M., Cohn, N., Anderson, D. L., and Serafin, K. A. (2017).
Extreme oceanographic forcing and coastal response due to the 2015–2016
El Niño. *Nature Communications*, 8:14365.
- Blaise, E., Suanez, S., Stephan, P., Fichaut, B., David, L., Cuq, V., Autret,
R., Houron, J., Rouan, M., Floc’h, F., Ardhuin, F., Cancouet, R., David-
son, R., Costa, S., and Delacourt, C. (2015). Review of winter storms
2013–2014 on shoreline retreat dynamic on Brittany coast. *Geomorpholo-
gie : Relief, Processus, Environnement*, 21(3):267–292.
- Boudière, E., Maisondieu, C., Ardhuin, F., Accensi, M., Pineau-Guillou, L.,
and Lepesqueur, J. (2013). A suitable metocean hindcast database for

438 the design of Marine energy converters. *International Journal of Marine*
439 *Energy*, 3–4:e40–e52.

440 Brenner, O. T., Lentz, E. E., Hapke, C. J., Henderson, R. E., Wilson, K. E.,
441 and Nelson, T. R. (2018). Characterizing storm response and recovery
442 using the beach change envelope: Fire Island, New York. *Geomorphology*,
443 300:189–202.

444 Bromirski, P. D. and Cayan, D. R. (2015). Wave power variability and trends
445 across the North Atlantic influenced by decadal climate patterns. *Journal*
446 *of Geophysical Research: Oceans*, 120(5):3419–3443.

447 Burvingt, O., Masselink, G., Scott, T., Davidson, M., and Russell, P. (2018).
448 Climate forcing of regionally-coherent extreme storm impact and recovery
449 on embayed beaches. *Marine Geology*, 401:112–128.

450 Castelle, B., Bujan, S., Ferreira, S., and Dodet, G. (2017a). Foredune mor-
451 phological changes and beach recovery from the extreme 2013/2014 winter
452 at a high-energy sandy coast. *Marine Geology*, pages 41–55.

453 Castelle, B., Dodet, G., Masselink, G., and Scott, T. (2017b). A new climate
454 index controlling winter wave activity along the Atlantic coast of Europe:
455 the West Europe Pressure Anomaly. *Geophysical Research Letters*, page
456 2016GL072379.

457 Castelle, B., Mariou, V., Bujan, S., Splinter, K., Robinet, A., Sénéchal, N.,
458 and Ferreira, S. (2015). Impact of the winter 2013-2014 series of severe
459 Western Europe storms on a double-barred sandy coast: Beach and dune
460 erosion and megacusp embayments. *Geomorphology*, 238:135–148.

461 Cazenave, A. and Cozannet, G. L. (2014). Sea level rise and its coastal
462 impacts. *Earth’s Future*, 2(2):15–34.

463 Davidson, M., Splinter, K., and Turner, I. L. (2013). A simple equilibrium
464 model for predicting shoreline change. *Coastal Engineering*, 73:191–202.

465 Davidson, M. A. and Turner, I. L. (2009). A behavioral template beach
466 profile model for predicting seasonal to interannual shoreline evolution.
467 *Journal of Geophysical Research: Earth Surface*, 114(F1):F01020.

468 Dodet, G., Bertin, X., and Taborda, R. (2010). Wave climate variability in
469 the North-East Atlantic Ocean over the last six decades. *Ocean Modelling*,
470 31(3–4):120–131.

471 Donat, M. G., Renggli, D., Wild, S., Alexander, L. V., Leckebusch,
472 G. C., and Ulbrich, U. (2011). Reanalysis suggests long-term upward
473 trends in European storminess since 1871. *Geophysical Research Letters*,
474 38(14):n/a–n/a.

475 Fernández-Mora, A., Calvete, D., Falqués, A., and de Swart, H. E. (2015).
476 Onshore sandbar migration in the surf zone: New insights into the wave-
477 induced sediment transport mechanisms. *Geophysical Research Letters*,
478 42(8):2014GL063004.

479 Ferreira, O. (2006). The role of storm groups in the erosion of sandy coasts.
480 *Earth Surface Processes and Landforms*, 31(8):1058–1060.

481 Hoefel, F. and Elgar, S. (2003). Wave-Induced Sediment Transport and
482 Sandbar Migration. *Science*, 299(5614):1885–1887.

483 Houser, C. and Hamilton, S. (2009). Sensitivity of post-hurricane beach and
484 dune recovery to event frequency. *Earth Surface Processes and Landforms*,
485 34(5):613–628.

486 Kalnay, E., Kanamitsu, M., Kistler, R., Collins, W., Deaven, D., Gandin,
487 L., Iredell, M., Saha, S., White, G., Woollen, J., Zhu, Y., Leetmaa, A.,
488 Reynolds, R., Chelliah, M., Ebisuzaki, W., Higgins, W., Janowiak, J.,
489 Mo, K. C., Ropelewski, C., Wang, J., Jenne, R., and Joseph, D. (1996).
490 The NCEP/NCAR 40-Year Reanalysis Project. *Bulletin of the American*
491 *Meteorological Society*, 77(3):437–471.

492 Masselink, G., Castelle, B., Scott, T., Dodet, G., Suanez, S., Jackson, D.,
493 and Floc'h, F. (2016a). Extreme wave activity during 2013/2014 winter
494 and morphological impacts along the Atlantic coast of Europe. *Geophysical*
495 *Research Letters*, page 2015GL067492.

496 Masselink, G. and Pattiaratchi, C. B. (2001). Seasonal changes in beach mor-
497 phology along the sheltered coastline of Perth, Western Australia. *Marine*
498 *Geology*, 172(3):243–263.

499 Masselink, G., Scott, T., Poate, T., Russell, P., Davidson, M., and Conley,
 500 D. (2016b). The extreme 2013/14 winter storms: hydrodynamic forcing
 501 and coastal response along the southwest coast of England. *Earth Surface*
 502 *Processes and Landforms*, 41:378–391.

503 McCall, R. T., Van Thiel de Vries, J. S. M., Plant, N. G., Van Dongeren,
 504 A. R., Roelvink, J. A., Thompson, D. M., and Reniers, A. J. H. M. (2010).
 505 Two-dimensional time dependent hurricane overwash and erosion modeling
 506 at Santa Rosa Island. *Coastal Engineering*, 57(7):668–683.

507 Mentaschi, L., Voudoukas, M. I., Voukouvalas, E., Dosio, A., and Feyen,
 508 L. (2017). Global changes of extreme coastal wave energy fluxes trig-
 509 gered by intensified teleconnection patterns. *Geophysical Research Letters*,
 510 44(5):2416–2426.

511 Morton, R. A., Paine, J. G., and Gibeaut, J. C. (1994). Stages and Durations
 512 of Post-Storm Beach Recovery, Southeastern Texas Coast, U.S.A. *Journal*
 513 *of Coastal Research*, 10(4):884–908.

514 Pachauri, R. K., Allen, M. R., Barros, V. R., Broome, J., Cramer, W.,
 515 Christ, R., Church, J. A., Clarke, L., Dahe, Q., and Dasgupta, P. (2014).
 516 *Climate change 2014: synthesis report. Contribution of Working Groups*
 517 *I, II and III to the fifth assessment report of the Intergovernmental Panel*
 518 *on Climate Change*. IPCC.

519 Robinet, A., Castelle, B., Idier, D., Marieu, V., and Harley, M. D. (2017).
 520 On a reduced-complexity shoreline model combining cross-shore and along-
 521 shore processes. In *Coastal Dynamics*, pages 1853–1862, Helsingor, Den-
 522 mark.

523 Scott, T., Masselink, G., O Hare, T., Saulter, A., Poate, T., Russell, P.,
 524 Davidson, M., and Conley, D. (2016). The extreme 2013/2014 winter
 525 storms: Beach recovery along the southwest coast of England. *Marine*
 526 *Geology*, 382:224–241.

527 Splinter, K. D., Turner, I. L., Davidson, M. A., Barnard, P., Castelle, B., and
 528 Oltman-Shay, J. (2014). A generalized equilibrium model for predicting
 529 daily to interannual shoreline response. *Journal of Geophysical Research:*
 530 *Earth Surface*, 119(9):1936–1958.

531 Stephan, P., Suanez, S., and Fichaut, B. (2015). Long, Mid and Short-Term
532 Evolution of Coastal Gravel Spits of Brittany, France. In *Sand and Gravel*
533 *Spits*, Coastal Research Library, pages 275–288. Springer Cham.

534 Suanez, S., Cariolet, J.-M., and Fichaut, B. (2010). Monitoring of recent
535 morphological changes of the dune of Vougot Beach (Brittany, France) using
536 Differential GPS. *Shore and Beach*, 78(1):37–40.

537 Sutherland, J., Peet, A. H., and Soulsby, R. L. (2004). Evaluating the performance
538 of morphological models. *Coastal Engineering*, 51(8):917–939.

539 Thom, B. and Hall, W. (1991). Behaviour of beach profiles during accretion
540 and erosion dominated periods. *Earth Surface Processes and Landforms*,
541 16(2):113–127.

542 Tolman, H. L. (2014). User manual and system documentation of WAVE-
543 WATCH III version 4.18. *NOAA/NWS/NCEP/MMAB Technical Note*
544 *316*, (276):194.

545 Turner, I. L., Harley, M. D., Short, A. D., Simmons, J. A., Bracs, M. A.,
546 Phillips, M. S., and Splinter, K. D. (2016). A multi-decade dataset of
547 monthly beach profile surveys and inshore wave forcing at Narrabeen,
548 Australia. *Scientific Data*, 3:160024.

549 van Rijn, L. C., Walstra, D. J. R., Grasmeijer, B., Sutherland, J., Pan, S.,
550 and Sierra, J. P. (2003). The predictability of cross-shore bed evolution of
551 sandy beaches at the time scale of storms and seasons using process-based
552 Profile models. *Coastal Engineering*, 47(3):295–327.

553 Vitousek, S., Barnard, P. L., Limber, P., Erikson, L., and Cole, B. (2017).
554 A model integrating longshore and cross-shore processes for predicting
555 long-term shoreline response to climate change. *Journal of Geophysical*
556 *Research: Earth Surface*, page 2016JF004065.

557 Wiggins, M., Scott, T., Masselink, G., Russell, P., Castelle, B., and Dodet,
558 G. (2017). The role of multi-decadal climate variability in controlling
559 coastal dynamics: re-interpretation of the ‘lost village of Hallsands’. pages
560 96–107, Helsingor.

- 561 Yates, M. L., Guza, R. T., and O'Reilly, W. C. (2009). Equilibrium shoreline
562 response: Observations and modeling. *Journal of Geophysical Research:*
563 *Oceans*, 114(C9):C09014.
- 564 Yates, M. L., Guza, R. T., O'Reilly, W. C., Hansen, J. E., and Barnard,
565 P. L. (2011). Equilibrium shoreline response of a high wave energy beach.
566 *Journal of Geophysical Research: Oceans*, 116(C4):C04014.

Table 1: Summary of beach site characteristics. $\tan\beta$ is the intertidal slope and MSR stands for mean spring tide range

Name	Region	Exposure	Hinterland	$D_{50}(\text{mm})$	$\tan\beta$	MSR (m)
Perranporth	Cornwall, UK	W Exposed	Dunes	0.35	0.015	4.5
Slapton	Devon, UK	SE Semi-sheltered	Lagoon	2-8	0.1	4.3
Vougout	Brittany, France	NNW Semi-exposed	Dunes	0.2-0.3	0.03	8.5
Porsmilin	Brittany, France	S Semi-shelterd	Seawall, Marsh	0.32	0.05	5.7
Truc Vert	Aquitaine, France	W Exposed	Dunes	0.4	0.025	3.9

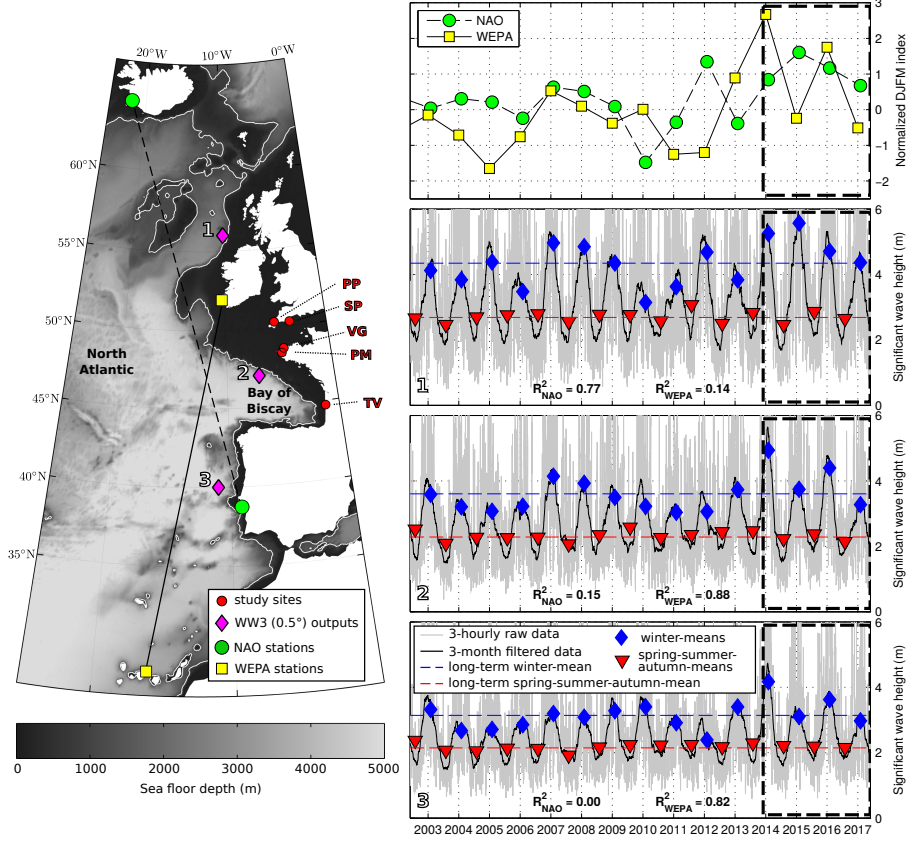


Figure 1: (left) Location map of the Atlantic coast of Europe showing the offshore bathymetry (greyscale), virtual wave buoys (pink diamonds), beach study sites Perranporth (PP), Slapton Sands (SP), Vougot (VG), Porsmilin (PM), Truc Vert (TV) (red circles), and weather stations used to compute the NAO (green circles) and WEPA indices (yellow squares). The white contour line represents the 1000 m isobath. (right) Time series of NAO and WEPA indices (top panel), and time series of raw (grey line), 3-month filtered (black line), winter-mean (blue diamond) and spring-summer-autumn mean (red triangles) significant wave height at the virtual buoys 1, 2 and 3 (bottom 3 panels). The dashed rectangle indicates the 2013/14 winter and the 4-year recovery period that followed. Squared correlation coefficients (R^2) between winter-mean H_s and NAO and WEPA indices are provided for each virtual buoy.

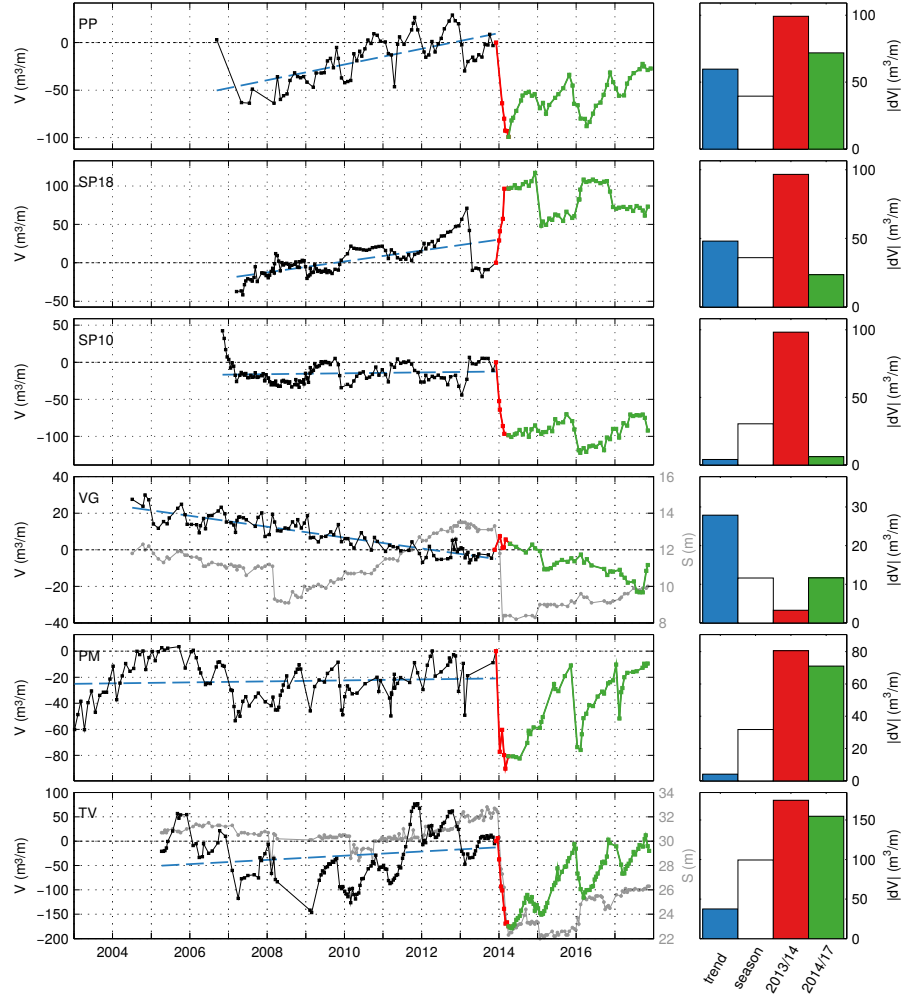


Figure 2: (left) Time series of beach volume at the five study sites (with two profiles shown for Slapton Sands), with the beach volume set to zero on December 1 2013. The dashed blue line represents the long-term trend over the period prior to the 2013/14 winter, the red line represents the 2013/14 winter response, and the green line represents the recovery period. For Vougot and Truc Vert the evolution of the location of the dune foot (grey line) is also shown. (right) Absolute values of the volume change associated with the long-term trend (blue), seasonal variability (white), 2013/14 winter response (red), and recovery period (green).

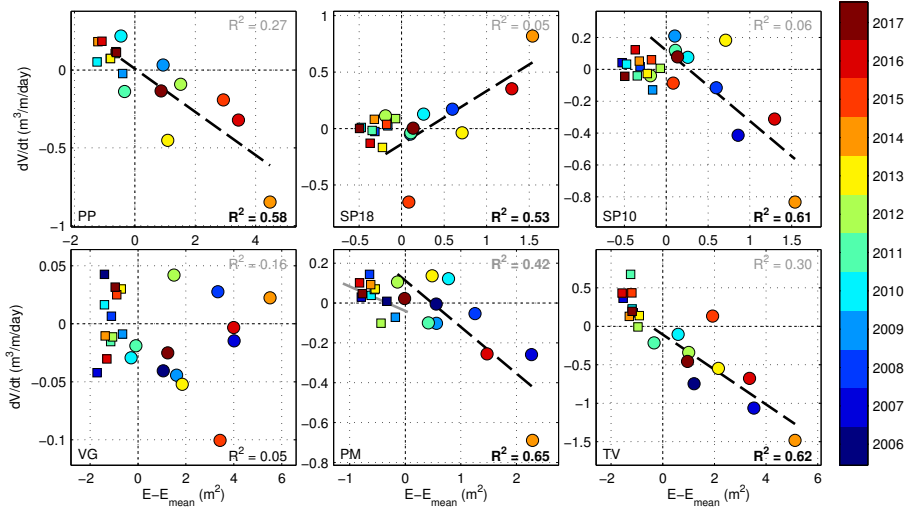


Figure 3: Beach volume changes during winter (circles) and summer-spring-autumn (squares) versus the wave energy anomaly (computed as the deviation of the season-mean wave energy from the long-term (1992–2017) annual mean wave energy), with colors indicating years. The squared correlation coefficients between beach volume changes and wave energy anomaly are given for winter (black) and spring-summer-autumn (grey). Linear regressions for winter (dashed light grey) and summer-spring-autumn (dashed dark grey) are plotted when the correlation is statistically significant at the 95 % level (in that case R^2 is written in bold).

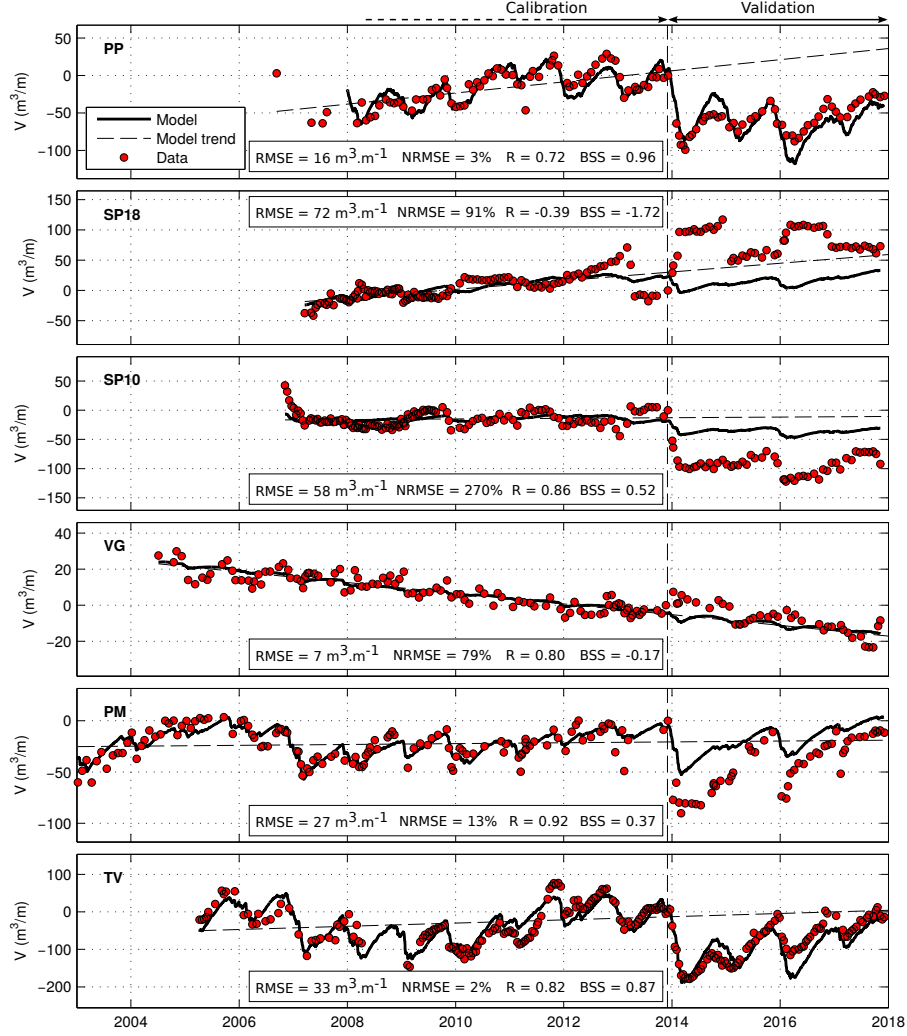


Figure 4: Comparison between ShoreFor model results and observations. Statistical errors are given for the validation period (post-2013/14 winter), and include the root-mean-square error (RMSE), the root-mean-square error normalized by the observed variance ($NRMSE$), the correlation coefficient (R) and the Brier Skill Score (BSS), with the long-term trend (dash black line) used as the baseline.